Kardar-Parisi-Zhang equation with spatially correlated noise: A unified picture from nonperturbative renormalization group

Thomas Kloss,[1] Léonie Canet,[2] Bertrand Delamotte,[3,4] and Nicolás Wschebor[3,4,5]

[1]*International Institute of Physics, UFRN, Av. Odilon Gomes de Lima 1722, 59078-400 Natal, Brazil*

[2]*LPMMC, CNRS UMR 5493, Université Joseph Fourier Grenoble, Boîte Postale 166, 38042 Grenoble, France*

[3]*Sorbonne Universités, UPMC Univ. Paris 06, UMR 7600, LPTMC, F-75005 Paris, France*

[4]*CNRS, UMR 7600, LPTMC, F-75005 Paris, France*

[5]*Instituto de Física, Facultad de Ingeniería, Universidad de la República, J.H.y Reissig 565, 11000 Montevideo, Uruguay*

(Received 20 December 2013; published 10 February 2014)

We investigate the scaling regimes of the Kardar-Parisi-Zhang (KPZ) equation in the presence of spatially correlated noise with power-law decay $D(p) \sim p^{-2\rho}$ in Fourier space, using a nonperturbative renormalization group approach. We determine the full phase diagram of the system as a function of ρ and the dimension d. In addition to the weak-coupling part of the diagram, which agrees with the results from Europhys. Lett. **47**, 14 (1999) and Eur. Phys. J. B **9**, 491 (1999), we find the two fixed points describing the short-range- (SR) and long-range- (LR) dominated strong-coupling phases. In contrast with a suggestion in the references cited above, we show that, for all values of ρ, there exists a unique strong-coupling SR fixed point that can be continuously followed as a function of d. We show in particular that the existence and the behavior of the LR fixed point do not provide any hint for 4 being the upper critical dimension of the KPZ equation with SR noise.

DOI: 10.1103/PhysRevE.89.022108 PACS number(s): 64.60.Ht, 05.10.Cc, 68.35.Ct, 68.35.Rh

I. INTRODUCTION

To describe interface roughening and its dynamical scaling, Kardar, Parisi, and Zhang (KPZ) proposed a nonlinear Langevin equation, which has now emerged as a fundamental model to study nonequilibrium phase transitions and scaling phenomena [1–4]. The KPZ equation [1] is written as follows:

$$\frac{\partial h(t,\vec{x})}{\partial t} = \nu\,\nabla^2 h(t,\vec{x}) + \frac{\lambda}{2}\,(\nabla h(t,\vec{x}))^2 + \eta(t,\vec{x}), \qquad (1)$$

where $h(t,\vec{x})$ is a single valued height profile which depends on the d-dimensional spatial coordinate $\vec{x}$ of the substrate and on time t, ν is the surface tension, and $\eta(t,\vec{x})$ represents a Gaussian noise with zero mean $\langle\eta(t,\vec{x})\rangle = 0$ and variance

$$\langle\eta(t,\vec{x})\eta(t',\vec{x}')\rangle = 2\,\mathcal{D}(\vec{x}-\vec{x}')\,\delta(t-t'). \qquad (2)$$

The nonlinear term proportional to λ is the essential ingredient to capture the dynamical roughening of the interface [2–4].

The original KPZ equation is formulated with a purely local noise of amplitude D, that is, $\mathcal{D}(\vec{x}-\vec{x}') = D\delta^d(\vec{x}-\vec{x}')$. This equation encompasses the following behavior. It always generates scaling in the stationary regime, characterized by the dynamical z and the roughness χ critical exponents. For dimensions $d \leqslant 2$, the interface always roughens, whereas for $d > 2$, a nonequilibrium phase transition occurs for a critical value λ_c of the nonlinearity, which separates a strong-coupling ($\lambda > \lambda_c$) rough phase from a weak-coupling ($\lambda < \lambda_c$) smooth phase corresponding to the linear Edwards Wilkinson (EW) regime, with exponents $z = 2$ and $\chi = (d-2)/2$. The ubiquity of the KPZ universality class has led to considerable efforts over the past decades to understand its statistical properties [2,3]. We do not review here all the corresponding literature but only mention the most recent contributions. For one-dimensional interfaces, an impressive breakthrough has been achieved during the past few years both theoretically [5–10] (and for a review, see, e.g., Ref. [11]) and experimentally [12–14]. For higher-dimensional interfaces, recent large-scale numerical simulations were launched to refine the estimates of critical exponents and probability distributions [15–19]. However, the progress is much slower, leaving still unsettled debates such as the existence of an upper critical dimension for this model.

Recently, we proposed a nonperturbative renormalization group (NPRG) approach for the KPZ equation [20–22], which successfully yielded the fully attractive [short-range (SR)] strong-coupling fixed point describing the rough phase in all dimensions. The associated exponents are in close (respectively, reasonable) agreement in $d = 2$ (respectively, $d = 3$) with the estimates from numerical simulations [15,16,23–28]. The finding of the fully attractive strong-coupling fixed point allows one to show the emergence of generic scaling for the two-point correlation and response functions. The resulting scaling functions in $d = 1$ compare remarkably well with the exact results [5,21]. These calculations have been extended in any dimensions, giving in particular the two-point correlation and response functions in $d = 2$ and $d = 3$ [22]. The ensuing predictions for the associated universal amplitude ratios in $d = 2$ have been recently accurately confirmed in lattice simulations [18].

We here address the issue of the presence of long-range (LR) correlated noise in the KPZ equation. Some experimental realizations (such as wetting in porous media [29,30]) have suggested that spatial correlations may exist at the microscopic level, in the noise or in the hydrodynamical interactions [2–4]. This has triggered the study of the relevance of this type of microscopic correlation, with regard to its impact on the critical exponents and on the phase diagram. Several numerical and theoretical studies have shown that spatial [31–43] and/or temporal [44–47] noise correlations indeed lead to new phases with modified exponents. Following Refs. [38–40,44], we consider, in addition to the local δ-correlated SR noise, a spatially correlated noise of the form

$$\mathcal{D}_{\rm LR}(\vec{x}-\vec{x}') \sim |\vec{x}-\vec{x}'|^{2\rho-d}, \quad \rho \leqslant d/2. \qquad (3)$$

More precisely, the full noise term in Fourier space is written as follows:

$$\mathcal{D}(\vec{p}) = D(1 + wp^{-2\rho}), \tag{4}$$

where $p = |\vec{p}|$ and w is the relative amplitude of the LR noise.

The early dynamical renormalization group (DRG) analysis by Medina *et al.* [44] predicted the existence of a rough LR-dominated phase above a threshold value of the decay exponent ρ of the LR noise, with associated ρ-dependent critical exponents $\chi = (2 - d + 2\rho)/3$ and $z = 2 - \chi$. This prediction was confirmed by a functional RG calulcation for directed polymers [48]. Yet some other theoretical approaches, based on a replica scaling analysis [49] or on a scaling analysis in open dissipative systems [32], yielded alternative predictions for the critical exponents and the threshold value of ρ. As early numerical simulations, mainly in one dimension, were not in accordance, the situation was unclear. However, later simulations [50] of the Burgers equation in $d = 1$ clearly confirmed the original DRG results, which were then also supported by a mode-coupling calculation [51], a self-consistent expansion [40,43] (at least in $d = 1$), and exact results from a DRG calculation using a stochastic Cole-Hopf transformation by Janssen, Frey, and Täuber (JFT) [38,39]. We present below the findings of JFT, which will serve as a reference for later comparison with our work.

JFT have shown that, in the presence of LR noise, new LR-dominated weak-coupling phases exist. They also suggested the existence of a LR-dominated strong-coupling phase even if the perturbative analysis cannot find the associated fixed point. Furthermore, they derived exact (i.e., valid to all orders in perturbation theory) expressions for the corresponding ρ-dependent exponents, including the LR-dominated strong-coupling phase (under the assumption that the associated fixed-point exists), which coincide with the DRG one-loop result. The physical picture emerging from their work is as follows. Below a lower critical dimension $d_c(\rho) = 2(1 + \rho)$, no smooth phase is stable, that is, the interface is always rough and the LR noise is either irrelevant at moderate ρ [$\rho < \rho_{\rm SR}(d)$] or dominates at larger ρ [$\rho > \rho_{\rm SR}(d)$]. The computation of $\rho_{\rm SR}(d)$ is not accessible perturbatively but is approximated by JFT by a linear interpolation between the exact result $(\rho,d) = (1/4,1)$ and the point $(\rho,d) = (1,4)$, deduced from a mapping to the Burgers equation with nonconserved noise (however, see below). Above $d_c(\rho)$, the two phases, smooth and rough, exist and JFT find that the LR noise is always relevant in the smooth phase while it is always irrelevant in the rough phase. From their results, they infer that the upper critical dimensions of the roughening transition and of the SR rough phase below $d_c(\rho)$ are $d = 4$. JFT also conjecture that the SR rough phases above and below $d_c(\rho)$ may be of two different natures (called SR-I and SR-II in their paper), with possibly different upper critical dimensions [38,39].

In the present paper, we revisit the work by JFT using the NPRG approach, successfully developed for the (SR noise) KPZ equation [20–22] and here generalized to include Gaussian LR correlated noise. We derive the corresponding NPRG flow equations at the next-to-leading order (NLO) approximation of Ref. [22] and solve them to determine the full phase diagram of the system for various values of ρ and d. Our results are in close agreement with the results of JFT in the weak-coupling sector. We recover in particular the smooth LR phases predicted above $d_c(\rho)$ with their exact critical exponents and correction-to-scaling exponents. Furthermore, we find the two stable fixed-point solutions in the strong-coupling regime (in their respective existence domain), describing the SR and the LR rough phases, with the exact LR exponents, and we compute the stability boundary line $\rho_{\rm SR}(d)$. The obtention of the complete phase diagram of the system in the (ρ,d) plane with all the expected fixed points constitutes our main result. In particular, we find that there exists a unique strong-coupling fixed point describing the SR rough phase in all dimensions, which is not consistent with the conjecture by JFT of the existence of two different rough phases SR-I and SR-II above and below $d_c(\rho)$. Furthermore, we investigate the phase diagram in the strong-coupling regime around $d = 4$, at least qualitatively since the NLO approximation is no longer accurate in this regime for $d \gtrsim 3.5$. Combining our findings and critical exponents from numerical simulations [16,24–26,52], we argue that $d = 4$ may not necessarily be the upper critical dimension of the SR rough phase. However, as the value of the SR roughness exponent in $d = 4$ cannot be reliably determined at this level of approximation, we cannot conclude yet about the actual value of d_c within NPRG, which requires a higher-order approximation and is left for future investigation.

The remainder of the paper is organized as follows. In Sec. II, we briefly present the NPRG formalism for the KPZ equation, including LR-correlated Gaussian noise and the approximations used. We then derive the corresponding flow equations. These equations are numerically integrated in Sec. III, and the full phase diagram of the system is determined and presented, including a discussion about the upper critical dimension.

II. NONPERTURBATIVE RENORMALIZATION GROUP

A. KPZ field theory and symmetries

The field theory associated with the KPZ equation (1) with both SR noise and Gaussian LR-correlated noise is derived in Ref. [38], following the Janssen-de Dominicis procedure [53]. The KPZ dynamic generating functional is given by

$$\mathcal{Z}[j,\tilde{j}] = \int \mathcal{D}[h,i\tilde{h}]\, \exp\left(-\mathcal{S}[h,\tilde{h}] + \int_{\mathbf{x}} \{jh + \tilde{j}\tilde{h}\}\right), \tag{5a}$$

$$\mathcal{S}[h,\tilde{h}] = \int_{\mathbf{x}} \left\{\tilde{h}(\mathbf{x})\left(\partial_t h(\mathbf{x}) - \nu\,\nabla^2 h(\mathbf{x}) - \frac{\lambda}{2}\,(\nabla h(\mathbf{x}))^2\right)\right\} - \int_{\mathbf{q}} \{D\,\tilde{h}(-\mathbf{q})(1 + wq^{-2\rho})\tilde{h}(\mathbf{q})\}, \tag{5b}$$

where $\tilde{h}$ is the Martin-Siggia-Rose response field [54], j and $\tilde{j}$ are sources, and the notation $\mathbf{x} \equiv (t,\vec{x})$, $\mathbf{q} \equiv (\omega,\vec{q})$ was introduced.

The symmetries of the KPZ action with correlated noise are twofold: (i) the h-shift symmetry and (ii) the Galilean symmetry. The additional discrete time-reversal symmetry of the one-dimensional SR KPZ equation is no longer realized in the presence of correlated noise. Moreover, as in the SR KPZ case, the symmetries (i) and (ii) are gauged in time [21,55] and

correspond to the following infinitesimal field transformations:

$$\text{(i)} \quad \begin{cases} h'(t,\vec{x}) = \vec{x}\cdot\partial_t\vec{v}(t) + h(t,\vec{x}+\lambda\vec{v}(t)) \\ \tilde{h}'(t,\vec{x}) = \tilde{h}(t,\vec{x}+\lambda\vec{v}(t)) \end{cases}, \tag{6a}$$

$$\text{(ii)} \quad h'(t,\vec{x}) = h(t,\vec{x}) + c(t). \tag{6b}$$

where $c(t)$ and $\vec{v}(t)$ are arbitrary infinitesimal time-dependent quantities. The variations of the KPZ action (5b) under these time-gauged transformations are linear in the fields and thus entail simple Ward identities, with a stronger content than the usual nongauged ones [21]. The detailed analysis of these symmetries is at the heart of the construction of the NPRG approximation scheme, derived in Ref. [21].

B. NPRG formalism

The general NPRG formalism for nonequilibrium systems is presented in Refs. [56–58], and its specific application to the KPZ equation in Ref. [21]. We only recall here the main elements, following Ref. [21]. In the spirit of Wilson's RG ideas, the NPRG formalism consists in building a sequence of scale-dependent effective models such that fluctuations are smoothly averaged as the (momentum) scale κ is lowered from the microscopic scale Λ, where no fluctuations are yet included, to the macroscopic scale $\kappa = 0$, where they are all summed over [59,60]. For classical nonequilibrium problems, one formally proceeds as in equilibrium, but with the presence of the response field, and additional requirements stemming from Itō's discretization and causality issues [56,61].

To achieve the separation of fluctuation modes within the NPRG procedure, one adds to the original action $\mathcal{S}$ a momentum and scale-dependent masslike term as follows:

$$\Delta\mathcal{S}_\kappa = \frac{1}{2}\int_{\mathbf{q}} h_i(-\mathbf{q})\,[R_\kappa(\mathbf{q})]_{ij}\,h_j(\mathbf{q}), \tag{7}$$

where the indices $i,j \in \{1,2\}$ label the field and response field, respectively $h_1 = h, h_2 = \tilde{h}$, and summation over repeated indices is implicit. The matrix elements $[R_\kappa(\mathbf{q})]_{ij}$ are proportional to a cutoff function $r(q^2/\kappa^2)$, with $q = |\vec{q}|$, which ensures the selection of fluctuation modes: $r(x)$ is required to almost vanish for $x \gtrsim 1$ such that the fluctuation modes $h_i(q \gtrsim \kappa)$ are unaffected by $\Delta\mathcal{S}_\kappa$, and to be large when $x \lesssim 1$ such that the other modes ($h_i(q \lesssim \kappa)$) are essentially frozen. Furthermore, $\Delta\mathcal{S}_\kappa$ must preserve all the symmetries of the problem and causality properties. As advocated in Ref. [21], an appropriate choice is

$$R_\kappa(\omega,\vec{q}) \equiv R_\kappa(\vec{q}) = r\left(\frac{q^2}{\kappa^2}\right)\begin{pmatrix} 0 & \nu_\kappa q^2 \\ \nu_\kappa q^2 & -2D_\kappa \end{pmatrix}, \tag{8}$$

where the running coefficients ν_κ and D_κ, defined later [Eq. (17)], are introduced in the regulator for convenience [20]. Here we choose the cutoff function

$$r(x) = \alpha/(\exp(x) - 1). \tag{9}$$

The dependence of our results on the parameter α is discussed in Appendix B.

In the presence of the mass term $\Delta\mathcal{S}_\kappa$, the generating functional (5a) becomes scale dependent,

$$\mathcal{Z}_\kappa[j,\tilde{j}] = \int \mathcal{D}[h,i\tilde{h}]\,\exp\left(-\mathcal{S} - \Delta\mathcal{S}_\kappa + \int_{\mathbf{x}}\{jh + \tilde{j}\tilde{h}\}\right). \tag{10}$$

Field expectation values in the presence of the external sources j and $\tilde{j}$ are obtained from the functional $\mathcal{W}_\kappa = \log\mathcal{Z}_\kappa$ as

$$\varphi(\mathbf{x}) = \langle h(\mathbf{x})\rangle = \frac{\delta\mathcal{W}_\kappa}{\delta j(\mathbf{x})}, \quad \tilde{\varphi}(\mathbf{x}) = \langle\tilde{h}(\mathbf{x})\rangle = \frac{\delta\mathcal{W}_\kappa}{\delta\tilde{j}(\mathbf{x})}. \tag{11}$$

The effective action $\Gamma_\kappa[\varphi,\tilde{\varphi}]$ is defined as the Legendre transform of $\mathcal{W}_\kappa$ (up to a term proportional to R_κ) as follows [56,59,62]:

$$\Gamma_\kappa[\varphi,\tilde{\varphi}] + \mathcal{W}_\kappa[j,\tilde{j}] = \int j_i\varphi_i - \frac{1}{2}\int \varphi_i\,[R_\kappa]_{ij}\,\varphi_j. \tag{12}$$

The exact flow for $\Gamma_\kappa[\varphi,\tilde{\varphi}]$ is given by Wetterich's equation, which in Fourier space is written as follows [59,63]:

$$\partial_\kappa\Gamma_\kappa = \frac{1}{2}\,\mathrm{Tr}\int_{\mathbf{q}}\partial_\kappa R_\kappa G_\kappa, \tag{13}$$

where

$$G_\kappa = \left[\Gamma_\kappa^{(2)} + R_\kappa\right]^{-1} \tag{14}$$

is the full, that is, field-dependent, renormalized propagator of the theory. When κ is lowered from Λ to 0, Γ_κ interpolates between the microscopic model $\Gamma_{\kappa=\Lambda} = \mathcal{S}$ and the full effective action $\Gamma_{\kappa=0}$ that encompasses all the macroscopic properties of the system [56]. Of course, Eq. (13) cannot be solved exactly, and one has to resort to an appropriate approximation scheme, adapted to the specific model under study and in particular to its symmetries.

C. Approximations

1. Next-to-leading order (NLO) approximation

In Ref. [21], inspired by the previous work in equilibrium statistical mechanics of Refs. [64–66], an approximation scheme is devised, which consists in building an ansatz for Γ_κ explicitly preserving the gauged shift (6b) and gauged Galilean (6a) symmetries. The building blocks are the Galilean invariants $\tilde{\varphi}$, $\nabla^2\varphi$, the covariant time derivative $D_t\varphi \equiv \partial_t\varphi - (\nabla\varphi)^2/2$, combined with the operators $\tilde{D}_t \equiv \partial_t - \nabla\varphi\cdot\nabla$ and ∇^2. We work here in the rescaled theory, where $\nu = D = 1$ and $\lambda \to \sqrt{g_b} = \lambda D^{1/2}/\nu^{3/2}$. Within this scheme, the "second order" (SO) ansatz for Γ_κ writes

$$\begin{aligned}\Gamma_\kappa[\varphi,\tilde{\varphi}] = \int_{\mathbf{x}}\Big\{&\tilde{\varphi}\,f_\kappa^\lambda\big(-\tilde{D}_t^2,-\nabla^2\big)D_t\varphi - \tilde{\varphi}\,f_\kappa^D\big(-\tilde{D}_t^2,-\nabla^2\big)\tilde{\varphi} \\ &- \frac{1}{2}\big[\nabla^2\varphi f_\kappa^\nu\big(-\tilde{D}_t^2,-\nabla^2\big)\tilde{\varphi} \\ &+ \tilde{\varphi}\,f_\kappa^\nu\big(-\tilde{D}_t^2,-\nabla^2\big)\nabla^2\varphi\big]\Big\},\end{aligned} \tag{15}$$

where f_κ^X, $X \in \{\nu,D,\lambda\}$ are three running functions. It is a truncation at quadratic order in the response field $\tilde{\varphi}$, while the complete momentum and frequency dependence of the two-point functions is preserved. Note that infinite powers of the field itself are included through the covariant time derivatives $\tilde{D}_t$. At the bare level $\kappa = \Lambda$, and for purely local noise, one has $f_\Lambda^\lambda = f_\Lambda^\nu = f_\Lambda^D = 1$,

The SO flow equations for the functions f_κ^X, derived in Ref. [21], were integrated in the simpler one-dimensional case, where the additional time-reversal symmetry imposes that there remains only one independent running function. The scaling functions associated with the two-point correlation

function were computed and showed an impressive agreement with the exact results [5,21]. However, the integration of the SO flow equations in generic dimensions appears rather involved, and a further simplification was proposed in Ref. [22]. This approximation, referred to as NLO, consists in neglecting the frequency dependence of the three flowing functions $f_\kappa^X(\omega,\vec{p}) \to f_\kappa^X(\vec{p})$ within the loop integrals, that is, the right-hand side of the flow equations. The NLO flow equations can be found in Ref. [22], where they were integrated in $d = 2$ and $d = 3$ and the scaling functions associated with the two-point correlation and response functions were computed. The related prediction for a universal amplitude ratio in $d = 2$ was very recently confirmed with great accuracy in lattice simulations [18].

In the present paper, we work with LR noise at the NLO approximation. Moreover, we focus on zero external frequency, since we are merely interested in the phase diagram and in the critical exponents and not in the full scaling functions. The zero-frequency sector is decoupled from the nonvanishing frequency sector within the NLO approximation, and we denote $f_\kappa^X(\omega = 0,\vec{p}) \equiv f_\kappa^X(\vec{p})$ for simplicity. The inclusion of the noise Eq. (4) then simply amounts to the substitution

$$f_\kappa^D(\vec{p}) \to \mathcal{D}_\kappa(\vec{p}) = f_\kappa^D(\vec{p}) + w_\kappa\, p^{-2\rho} \tag{16}$$

(with bare condition $w_\Lambda = w$) in the NLO ansatz. The first term $f_\kappa^D(\vec{p})$ corresponds to the renormalized SR contribution at scale κ and the second term to the LR one. This separation in terms of a regular ($f_\kappa^D(\vec{p})$) and a nonanalytic ($w_\kappa p^{-2\rho}$) part holds for all κ because, as the flow is regularized in the IR and finite in the UV, it cannot generate nonanalytic contributions. Correspondingly, the nonanalytic part is not renormalized ($\partial_\kappa w_\kappa = 0$) and the coupling w_κ remains equal to its bare value. Thus, in the presence of LR noise, the NLO flow equations for the three functions f_κ^X are identical to those for the local SR case up to the substitution (16).

The gauged shift symmetry implies the nonrenormalization of $f_\kappa^\lambda(0)$ that therefore remains equal to unity for all κ. Moreover, the Galilean symmetry implies the nonrenormalization of the nonlinear coupling λ. We hence define two scale-dependent parameters D_κ and ν_κ as follows:

$$D_\kappa \equiv f_\kappa^D(0), \quad \nu_\kappa \equiv f_\kappa^\nu(0). \tag{17}$$

These two running coefficients yield two running anomalous dimensions, defined according to

$$\eta_\kappa^D = -\kappa\partial_\kappa \ln D_\kappa \quad \text{and} \quad \eta_\kappa^\nu = -\kappa\partial_\kappa \ln \nu_\kappa, \tag{18}$$

which fixed-point values, indexed by *, are related to the physical critical exponents by

$$z = 2 - \eta_*^\nu, \quad \chi = (2 - d + \eta_*^D - \eta_*^\nu)/2. \tag{19}$$

In order to study fixed-point properties, we introduce dimensionless quantities. The dimensionless couplings are

$$\hat{w}_\kappa = w_\kappa\, D_\kappa^{-1}\kappa^{-2\rho}, \tag{20a}$$

$$\hat{g}_\kappa = g_b\, \kappa^{d-2}\, D_\kappa/\nu_\kappa^3, \tag{20b}$$

and their flow equations, due to the nonrenormalization of w_κ and λ, are, hence, reduced to their dimensional parts as follows:

$$\partial_s \hat{w}_\kappa = \hat{w}_\kappa\big(\eta_\kappa^D - 2\rho\big), \tag{21a}$$

$$\partial_s \hat{g}_\kappa = \hat{g}_\kappa\big(d - 2 + 3\eta_\kappa^\nu - \eta_\kappa^D\big), \tag{21b}$$

with $\partial_s \equiv \kappa\partial_\kappa$. The dimensionless running functions are defined by

$$\hat{f}_\kappa^X(\hat{p}) = f_\kappa^X(p)/X_\kappa \tag{22}$$

for $X \in \{D,\nu,\lambda\}$ and $X_\kappa \in \{D_\kappa,\nu_\kappa,1\}$, and their flows write

$$\partial_s \hat{f}_\kappa^X(\hat{p}) = \eta_\kappa^X\, \hat{f}_\kappa^X(\hat{p}) + \hat{p}\ \partial_{\hat{p}} \hat{f}_\kappa^X(\hat{p}) + \hat{I}_\kappa^X(\hat{p}), \tag{23}$$

with $\hat{p} = p/\kappa$, $\eta_\kappa^X \in \{\eta_\kappa^D,\eta_\kappa^\nu,0\}$, and the $\hat{I}_\kappa^X(\hat{p})$ are the loop integrals, which explicit expressions are given in Ref. [22] up to the substitution (16).

The five flow equations [(21) and (23)] are solved numerically with Euler time stepping and $\Delta s = -4 \times 10^{-4}$ in the RG "time" s. The three flowing functions $\hat{f}_\kappa^X$ are set to unity at the initial scale $s = 0$. We observe that the flow always converges to a stable fixed point, which nature depends on the initial conditions for $\hat{g}_\Lambda = g_b$ and $\hat{w}_\Lambda$. From these flows, one then deduces the phase diagram in the $(\hat{g},\hat{w})$ plane for each value of the parameters (ρ,d), which is discussed in Sec. III.

2. *Local potential approximation*

As studied in detail in Ref. [22], the NLO approximation gives a reliable quantitative description of the SR fixed point up to $d \simeq 3.5$. However, the numerical cost to solve the coupled NPRG flow equations is high, especially as the flow, in the vicinity of unstable fixed points, slows down to an impractical time scale. To fully explore the phase diagram, it is therefore convenient to sometimes resort to an additional approximation, usually referred to as the local potential approximation prime (LPA′) [62], where only field-independent renormalization coefficients are kept. It thus consists in the following simplification:

$$\hat{f}_\kappa^X(\hat{p}) \to \hat{f}_\kappa^X(0) \equiv 1. \tag{24}$$

The LPA′ was shown to capture the qualitative structure of the phase diagram in the pure SR case, although the estimate for the critical exponents rapidly deteriorates as the dimension grows [67]. This approximation will be used to determine the weak-coupling part of the phase diagram. The complete NLO approximation is, however, necessary to study the boundary between the SR- and LR-dominated rough phases in $d = 2$ and 3. It indeed turns out that the value of the roughness exponent χ is overestimated at the LPA′, such that the stability change of the SR and LR fixed points is shifted to unphysical values where $\rho > d/2$ in this approximation, see Eq. (3). In the following, we will indicate whether the NLO or the LPA′ is used.

D. Change of variables

As found by JFT, the LR weak-coupling fixed points (EWLR1 and EWLR2, see below) describing the smooth phase when it exists have an infinite noise amplitude coordinate $\hat{w}_* = \infty$. It is therefore convenient to change variables such that the fixed-point coordinates remain finite. We choose the

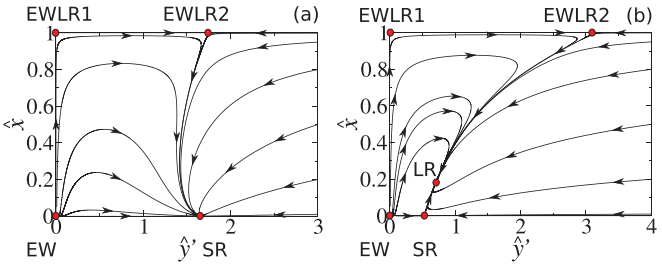

FIG. 1. (Color online) RG trajectories in the $(\hat{y}',\hat{x})$ plane in $d = 2$ for (a) $\rho = 0.3$ and (b) $\rho = 0.7$ obtained with the LPA′. Increasing ρ, the LR fixed point moves from the unphysical quadrant $\hat{x} < 0$ [not shown in panel (a)] to the physical one [panel (b)] through crossing the SR fixed point that thus simultaneously changes stability in the $\hat{y}'$ direction.

same variables as JFT [38,39], namely

$$\hat{x}_\kappa = \frac{\hat{w}_\kappa}{1+\hat{w}_\kappa}, \quad \hat{y}_\kappa = \frac{1}{4\rho}(1+\hat{w}_\kappa)^2\hat{g}_\kappa, \tag{25}$$

to simplify the comparison.

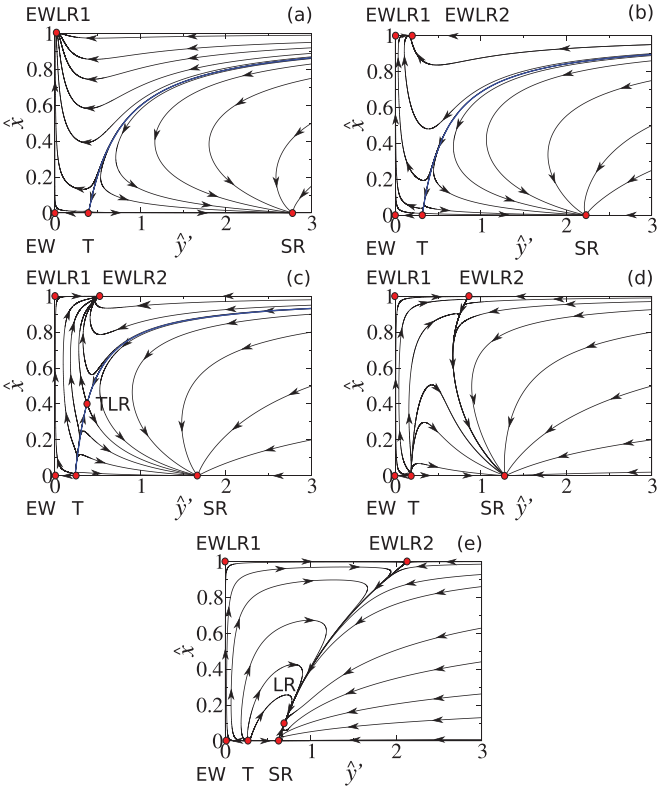

FIG. 2. (Color online) RG trajectories in the $(\hat{y}',\hat{x})$ plane in $d = 3$ for increasing values of ρ: (a) $\rho = 0.24$, (b) $\rho = 0.3$, (c) $\rho = 0.4$, (d) $\rho = 0.52$, (e) $\rho = 0.9$, obtained with the LPA′ for (a) to (d) and NLO for (e). Panels (a) and (b): The EWLR2 fixed point enters into the physical quadrant $\hat{y}' > 0$ and EWLR1 changes its stability. Panel (c): The TLR fixed point enters into the physical quadrant $\hat{x} > 0$ and T changes stability. Panel (d): The TLR fixed point merges with EWLR2 that changes stability. Panel (e): The LR fixed point enters into the physical quadrant $\hat{x} > 0$ and the SR fixed point changes stability.

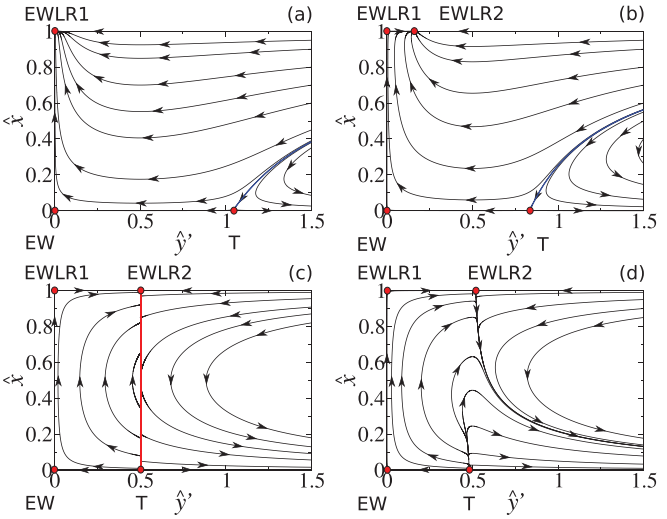

FIG. 3. (Color online) RG trajectories in the $(\hat{y}',\hat{x})$ plane in $d = 3$ and for increasing values of ρ: (a) $\rho = 0.24$, (b) $\rho = 0.3$, (c) $\rho = 0.5$, and (d) $\rho = 0.52$, obtained with the perturbative flow equations (A1). The rapid move of TLR in Fig. 2 is replaced by a fixed line joining T and EWLR2 displayed in (c), the rest of the (weak-coupling part of the) flow diagrams being very similar to the nonperturbative ones. (Note the difference of the $\hat{y}'$ scale.)

In terms of the new couplings $\hat{x}$ and $\hat{y}$, the flow equations (21) become

$$\partial_s \hat{x}_\kappa = \hat{x}_\kappa(1-\hat{x}_\kappa)\big(\eta_\kappa^D - 2\rho\big), \tag{26a}$$

$$\partial_s \hat{y}_\kappa = \hat{y}_\kappa\big(2\hat{x}_\kappa\big(\eta_\kappa^D - 2\rho\big) + d - 2 + 3\eta_\kappa^v - \eta_\kappa^D\big), \tag{26b}$$

where we have implicitly assumed that the anomalous dimensions η_κ^X, which depend on $\hat{g}_\kappa$ and $\hat{w}_\kappa$, are now expressed in terms of $\hat{x}_\kappa$ and $\hat{y}_\kappa$.

Let us finally define the variable $\hat{y}'_\kappa = v_d\hat{y}_\kappa/4$, where $v_d^{-1} = 2^{d-1}\pi^{d/2}\Gamma(d/2)$ is related to integration volume, which is used for graphical convenience in all the representations of flow diagrams, Figs. 1–4.

III. RESULTS

A. Fixed points

We study in the following the existence and stability of the fixed-point solutions of the NPRG flow equations (26) and (23)

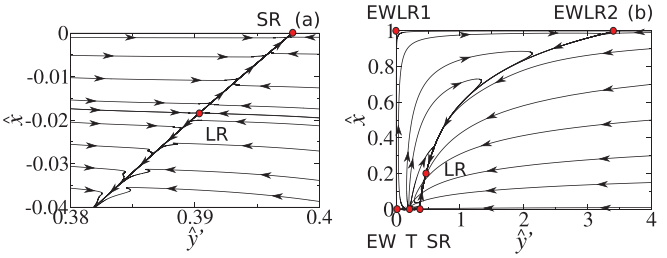

FIG. 4. (Color online) RG trajectories in the $(\hat{y}',\ \hat{x})$ plane in $d = 4$ for (a) $\rho = 1.125$ and (b) $\rho = 1.25$ obtained with NLO. The LR fixed point lies away from the Gaussian fixed point and is fully attractive for $\rho \gtrsim 1.14$.

as functions of d and ρ. Three fixed points correspond to a vanishing $\hat{g}_*$ and are thus referred to as Edwards-Wilkinson fixed points. One (denoted EW) is at $(\hat{x}_* = 0, \hat{y}_* = 0)$ while two others (EWLR1 and EWLR2) correspond to infinite $\hat{w}_*$, that is, $\hat{x}_* = 1$. Another fixed point, denoted T (for transition), exists at $\hat{x}_* = 0$ and $\hat{y}_* > 0$ (for $d > 2$) and separates at vanishing LR noise amplitude the smooth and rough phases. All these four fixed points were found perturbatively and their coordinates, stability, and associated exponents were obtained exactly in the Cole-Hopf representation of the theory [38]. Besides these fixed points, we find three others. Two, denoted SR and LR, describe the rough phase, respectively, when the LR noise is irrelevant and relevant. These fixed points are genuinely nonperturbative, that is, are not accessible at any order of the perturbative expansion. The last fixed point, denoted TLR (for transition in the presence of LR noise), exists in a (narrow) band of the (ρ,d) plane that separates, above the band, a region where there exists a transition between the smooth and rough phases, and below the band, a region where there is no stable smooth phase and where the long-distance physics is described by either SR or LR (when, initially, the amplitude of the noise is nonvanishing).

1. Edwards-Wilkinson fixed point

The EW fixed point corresponds to $(\hat{x}_*, \hat{y}_*) = (0,0)$, which implies $\eta^{\rm D}_* = \eta^{\nu}_* = 0$ and $\chi_{\rm EW} = (2-d)/2, \quad z_{\rm EW} = 2$. This fixed point is always unstable with respect to LR noise, i.e., in the $\hat{x}$ direction. It is repulsive (respectively, attractive) in the $\hat{g}$ (or $\hat{y}$) direction for $d \leqslant 2$ (respectively, $d > 2$).

2. EWLR1 fixed point

This fixed point is located at $(\hat{x}_*, \hat{y}_*) = (1,0)$. It is always attractive in the $\hat{x}$ direction while it is attractive (respectively, repulsive) for $d > d_{\rm EWLR}(\rho) = 2(1+2\rho)$ (respectively, for $d < d_{\rm EWLR}(\rho)$) in the $\hat{y}$ direction; see Appendix A. At this fixed point, $\eta^{\nu}_* = \eta^{\rm D}_* = 0$, and the exponents are $\chi_{\rm EWLR} = (2-d+2\rho)/2$ and $z_{\rm EWLR} = 2$. The associated correction-to-scaling exponents are $\omega_1 = 2\rho$ and $\omega_2 = d-2-4\rho$; see Appendix A.

3. EWLR2 fixed point

The EWLR2 fixed point exists for $d \leqslant d_{\rm EWLR}(\rho)$ [it coincides with EWLR1 at $d = d_{\rm EWLR}(\rho)$] and is located at $\hat{x}_* = 1$ and $\hat{y}_* \geqslant 0$; see Eq. (A14). It is always attractive in the $\hat{y}$ direction, while its stability in the $\hat{x}$ direction changes at $d = d_c(\rho) = 2(1+\rho)$, from unstable for $d < d_c(\rho)$ to stable for $d > d_c(\rho)$. The critical exponents $\chi_{\rm EWLR}$ and $z_{\rm EWLR}$ are identical in the two LR smooth phases. However, as already emphasized by JFT, they differ by their correction-to-scaling exponents, which are for EWLR2 $\omega_1 = d-2-2\rho$ and $\omega_2 = 4\rho - (d-2)$; see Appendix A.

4. Transition fixed point

The transition fixed point T exists for $d \geqslant 2$ at $\hat{x}_* = 0$ and $\hat{y}_* \geqslant 0$ (it coincides with EW in $d = 2$). It is always unstable in the $\hat{y}$ direction. In the Cole-Hopf representation, the change of stability of T in the $\hat{x}$ direction occurs exactly at $d = d_c(\rho)$ [or, equivalently, at $\rho_c(d) = (d-2)/2$], simultaneously with the change of stability of EWLR2, via the appearance of a line of fixed points joining the two fixed points [38]. Within our approximations, we find, at fixed d, that T is stable in the $\hat{x}$ direction at small ρ and that its stability changes at $\rho_c^T(d) = (d-2+3\chi_{\rm T})/2 \lesssim \rho_c(d)$ [or, equivalently, at $d_c^T(\rho)$] since the exact value for the critical exponent at the transition $\chi_{\rm T} = 0$ is only recovered approximately within our approximations. (Given that NLO and LPA′ are exact at one loop, we find, as expected, $\chi_{\rm T} = \mathcal{O}(\epsilon^2)$. However, when d grows, it becomes slightly negative rather than strictly vanishing).

5. TLR fixed point

This fixed point is found for $\rho_c^T(d) < \rho < \rho_c(d)$ [equivalently, for $d_c^T(\rho) > d > d_c(\rho)$] and has coordinates $\hat{x}_* > 0$ and $\hat{y}_* > 0$. It is unstable in the $\hat{y}$ direction and drives the transition between SR and EWLR2. As explained above, in the Cole-Hopf representation, the stabilities of the two fixed points T and EWLR2 are switched together through the appearance at $\rho = \rho_c(d)$ of a fixed line joining them. This feature is not preserved by our approximation. We find instead that at fixed d and upon increasing ρ, the TLR fixed point first crosses T at $\rho_c^T(d)$ and then travels up the entire plane $0 < \hat{x} < 1$ before eventually crossing EWLR2 at $\rho_c(d)$. The line of fixed points is thus replaced by the TLR fixed point which moves very rapidly between T and EWLR2 as ρ is increased. This feature is probably an artifact of our approximations (if the line of fixed points is an exact result, valid beyond perturbation theory). However, the flow is modified only in a narrow band between $\rho_c^T(d)$ and $\rho_c(d)$, and the physically observable phases remain unaffected, controlled by the fully attractive EWLR2 or SR fixed point (compare Figs. 2 and 3).

6. Short-range fixed point

The SR fixed point is located at $\hat{x}_* = 0$ and $\hat{y}_* > 0$. It exists in all dimensions and describes the rough (strong-coupling) phase of the KPZ equation without LR noise. Within all our approximations (except the LPA′), the associated exponents are in good agreement with the numerical ones in $d = 2$ and $d = 3$ [20–22]. The quality of our approximations deteriorates with increasing dimension and none of them yields reliable quantitative results above typically $d = 3.5$. In all dimensions we find that SR is stable in the $\hat{y}$ direction. Its stability in the noise direction can be inferred from Eqs. (19) and (26), that is,

$$\partial_s \hat{x}_\kappa = \hat{x}_\kappa(1-\hat{x}_\kappa)(d-2+3\chi_{\rm SR}-2\rho). \tag{27}$$

The sign change of the β function in the $\hat{x}$ direction hence occurs at

$$d_{\rm SR} = 2 + 2\rho - 3\chi_{\rm SR}. \tag{28}$$

At fixed d, the SR fixed point is attractive in the noise direction for $\rho < \rho_{\rm SR}(d) = (d-2+3\chi_{\rm SR})/2$ and becomes repulsive beyond this value.

7. Long-range fixed point

The LR fixed point has coordinates $\hat{x}_* > 0$ and $\hat{y}_* > 0$ and describes a strong-coupling rough, LR-dominated phase. At fixed d, it exists for $\rho > \rho_{\rm SR}(d)$ [it coincides with SR at $\rho = \rho_{\rm SR}(d)$] and is attractive in all directions. Under the assumption that it indeed exists, the associated exponents have

TABLE I. Location of the boundary line $\rho_{SR}(d)$ between the SR and LR phases as a function of the dimension d from JFT [38], NLO (this work, $\alpha = 4$, see Appendix B), and numerical simulations (mean values from Refs. [15,16,23–28]).

d	1	2	3	4
ρ_{SR}^{JFT}	1/4	1/2	3/4	1
ρ_{SR}^{NLO}	1/4	0.57	0.79	–
$\rho_{SR}^{num.}$	0.25	0.57	0.95	1.37

been determined exactly in the Cole-Hopf representation [38],

$$\chi_{LR} = (2 - d + 2\rho)/3, \quad z_{LR} = (4 + d - 2\rho)/3, \qquad (29)$$

and are also obtained exactly from the NPRG Eqs. (19) and (21) at any nontrivial fixed point with nonvanishing LR noise. Let us notice that the LPA′ is not sufficient to find with a reasonable accuracy the value of $\rho_{SR}(d)$, where SR and LR exchange their stability and we resorted to the complete NLO approximation to get it. We compare in Table I the location of the boundary line $\rho_{SR}(d)$ between the SR and LR phases obtained with different approaches. The JFT result corresponds to a linear interpolation $\rho_{SR}(d) = d/4$ proposed by these authors [38]. The NLO and the numerical results correspond to the value of ρ verifying $\chi_{LR} = \chi_{SR}$, that is, $\rho_{SR}(d) = (3\chi_{SR} + d - 2)/2$, where the values for χ_{SR} are obtained respectively from the NLO approximation or numerical simulations [15,16,23–28].

B. Discussion of the phase diagram

After having characterized all the fixed-point solutions of the NPRG flow equations, we now provide a complete picture of the phase diagram (see Fig. 5). There are two distinct situations depending on the dimension. First, we confirm the general picture found by JFT. That is, for $d < d_c(\rho)$, the interface is always rough, with a phase boundary $\rho_{SR}(d)$ separating the usual strong-coupling SR phase for $\rho < \rho_{SR}(d)$ and a LR-dominated phase with ρ-dependent critical exponents for $\rho > \rho_{SR}(d)$. Above $d_c(\rho)$, the T fixed point drives a transition between a smooth LR phase and a rough SR phase. In the following, we discuss the details of the phase diagram, reasoning rather at fixed d and for varying ρ, which is closer in spirit to what can be observed in simulations.

For $d \leqslant 2$, the system is always in a rough phase and for $\rho \leqslant \rho_{SR}(d)$ the flow is driven to the SR fixed point whatever the initial condition is, provided the nonlinearity is nonvanishing ($\lambda > 0$); see Fig. 1(a). In this case, the presence of the LR noise does not change the long distance physics of the KPZ equation. At $\rho = \rho_{SR}(d)$, the LR fixed point crosses SR and enters the physical quadrant $\hat{x} > 0$ for $\rho > \rho_{SR}(d)$. It is then fully attractive and drives the long-distance physics of any model showing nonvanishing LR noise; see Fig. 1(b).

For $d > 2$, the situation is more complex. At vanishing LR noise amplitude ($w_\Lambda = 0$), the fixed point T separates a smooth (at small g_Λ) and a rough (at large g_Λ) phase. The smooth phase is described by the usual EW fixed point and the rough phase by the SR fixed point. For $\rho < \rho_c(d) = (d - 2)/2$ and nonvanishing noise amplitudes, there exists a critical line

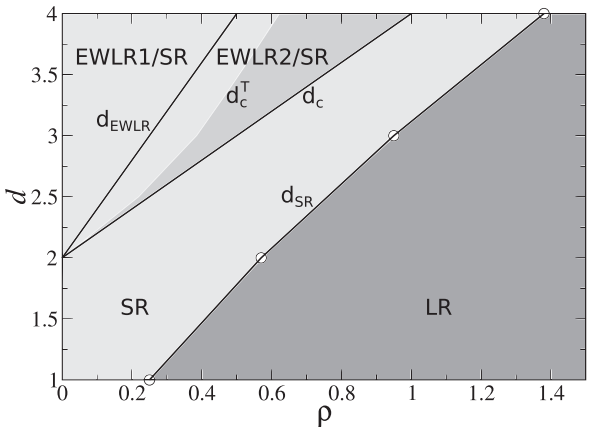

FIG. 5. Phase diagram of the KPZ equation with spatially LR-correlated noise in the (ρ,d) plane. Bounds between the regions, which are indicated by black lines, are given by $d_{EWLR}(\rho) = 2(1 + 2\rho)$, $d_c(\rho) = 2(1 + \rho)$ and $d_{SR}(\rho)$ defined by (28) where averaged values for χ_{SR} are taken from numerical simulations (mean values from Refs. [15,16,23–28]). LR is the unique fully attractive fixed point in the dark gray region. In the other regions there is either a phase transition between a smooth and a rough phase where the LR noise is irrelevant or, below $d_c(\rho)$, only a rough phase described by SR. The TLR fixed point exists in the gray region between the lines d_c^T and d_c; see Sec. III A 4.

(highlighted in blue in Figs. 2 and 3) ending at T also separating a smooth and a rough phase. This line is nontrivial as can be seen in Figs. 2(a)–2(c). Depending on ρ, the flow in the smooth phase is either driven, for $\rho < (d - 2)/4$ to EWLR1 [Fig. 2(a)] or for $(d - 2)/2 > \rho > (d - 2)/4$ to EWLR2 [Fig. 2(b)]. In the rough phase, the flow is driven to SR for $\rho < \rho_{SR}(d)$ [Figs. 2(a)–2(d)], which becomes fully attractive in the entire $(\hat{y}',\hat{x})$ plane for $\rho_c(d) < \rho < \rho_{SR}(d)$ [Figs. 2(d)]. In this case, the LR noise is irrelevant and the LR fixed point lies in the unphysical quadrant $\hat{x} < 0$. For $\rho > \rho_{SR}(d)$, the LR fixed point crosses SR and appears in the physical quadrant $\hat{x} > 0$ becoming the dominant, fully attractive fixed point [Fig. 2(e)]. For $\rho > \rho_c(d)$ and $d > 2$, the flow is thus very similar to what is found in $d \leqslant 2$: Either $\rho < \rho_{SR}(d)$ and SR is fully attractive or $\rho > \rho_{SR}(d)$ and LR is fully attractive and governs the rough phase. Let us emphasize that we can follow continuously all these fixed points in the (ρ,d) plane and that there are no two distinct SR phases contrary to what was conjectured in Ref. [38].

As already mentioned, if no approximations were performed and if one worked in the perturbative Cole-Hopf approach, a fixed line joining T to EWLR2 would appear exactly at $\rho = \rho_c(d)$ and for $\rho > \rho_c(d)$ both fixed points would become unstable; see Fig. 3. Instead, within our approximations and upon increasing ρ at fixed d, the unstable fixed point TLR crosses T for $\rho = \rho_c^T(d)$, moves very rapidly towards EWLR2, and, finally, crosses this fixed point at $\rho = \rho_c(d)$ [Figs. 2(c) and 2(d)], changing the stability of these fixed points upon crossing them. However, this little discrepancy does not modify qualitatively the rest of the phase diagram and the physically observable phases are unaffected (compare Figs. 2 and 3).

C. Discussion about the upper critical dimension

We have followed the LR fixed point up to dimension 4 for $\rho \simeq 1$ [68]. We observed that it does not lie close to the Gaussian fixed point near $\rho = 1$ and $d = 4 - \epsilon$. In fact, within the NLO approximation, we find in $d = 4$ that a transition between the SR- and LR-dominated phases occurs at $\rho_{\rm SR}(4) \simeq 1.14$, such that the LR fixed point becomes the stable fixed point for $\rho > \rho_{\rm SR}(4)$ with a finite value of $\hat{y}_*$, see Fig. 4. We recall that our results in the strong-coupling phase show a large dependence on the choice of regulators for dimensions larger than typically 3.5, which strongly suggests that our approximations are not accurate in this case; see Appendix B. However, there is no doubt that the LR fixed point cannot become Gaussian in $d = 4$ and $\rho = 1$. As a matter of fact, if it were Gaussian, it would exist as a solution of the perturbative expansion of our NPRG equations since our approximations, either the LPA$'$ or NLO, are exact at one-loop order by construction. There is no such a solution. To put it differently, while the strong-coupling regime of the problem becomes out of reach of our approximations in large dimensions, the weak-coupling regime remains under control. In the NPRG calculations, the case $d = 4$ and $\rho = 1$ does *not* map onto the Burgers equation with nonconserved noise (i.e., model B of Forster *et al.* [69] applied to the Burgers equation). In the latter, only a LR noise is present and it does not include a SR part, such that nothing can be inferred from this model about the stability of the LR fixed point against a SR component. The reason for the discrepancy with JFT who advocated this mapping is that, in the RG approach, the SR noise is generated by the flow even if it is not present initially and it cannot be neglected. The full complexity of the KPZ equation with both types of noise, and their competition, cannot be avoided to determine their respective relevance. As a result, the usual power counting argument performed in model B (for LR $\rho = 1$ without a SR component) leading to an upper critical dimension of 4 for LR cannot be applied here.

Within the NPRG framework, as already mentioned, the NLO approximation is not accurate above $d \simeq 3.5$. However, the qualitative structure of the obtained phase diagram in $d = 4$ in the strong-coupling sector (Fig. 4), together with some inputs from numerical simulations for the critical exponent, open up another possibility, which we now stress. The stability exchange between SR and LR proceeds when LR comes across SR from below, which occurs for $\chi_{\rm SR} = \chi_{\rm LR}$. Thus, if $\chi_{\rm SR} > 0$ in $d = 4$, as suggested by numerical simulations, SR appears as the stable fixed point for $\rho = 1$, dominating over LR, which has $\chi_{\rm LR} = 0$ and still lies in the unphysical quadrant $\hat{x} < 0$ of the coupling constant space (see Fig. 5). From simulation results for $\chi_{\rm SR}$, the SR stability change in $d = 4$ occurs around $\rho_{\rm SR} \simeq 1.38$, and thus SR is still fully attractive at $\rho = 1$ [16,24–26,52].

Let us summarize the previous discussions of the phase diagram and of $d = 4$. We emphasized that the existence of two different types of SR phases above and below $d_c(\rho)$ with different upper critical dimensions is not consistent with our finding of a unique SR fixed point. However, we proposed an alternative scenario which could reconcile numerical simulations and RG analysis, namely that the LR fixed point is unstable against SR at $d = 4$ and $\rho = 1$. Let us emphasize once more that we cannot settle yet whether this scenario is realized within NPRG, i.e., whether $\chi_{\rm SR}$ is vanishing in $d = 4$. Doing so requires a higher-order approximation, and this issue will be addressed in future work.

IV. CONCLUSION

In the present work, we investigated, using NPRG, the phase diagram of the KPZ equation with Gaussian LR correlated noise with power-law decaying correlator $\mathcal{D}(p) = D(1 + wp^{-2\rho})$ in Fourier space. We generalized the NPRG flow equations in the NLO approximation to include LR noise. We then integrated them numerically to determine the complete phase diagram of this model as a function of d and ρ and confronted it with the results obtained by JFT, which are valid to all orders in perturbation theory.

In the weak-coupling sector, the two approaches are in close agreement. We recover in particular that above $d_c(\rho) = 2(1 + \rho)$, the smooth phase is LR dominated and is controlled by one of the two weak-coupling LR fixed points EWLR1 or EWLR2, with their exact critical exponents and correction-to-scaling exponents. One difference appears between the two approaches: the line of fixed point joining T and EWLR2 at exactly $\rho_c(d) = (d - 2)/2$ is replaced in the NPRG approach at NLO by an unstable fixed point TLR rapidly moving from T to EWLR2 as ρ is increased in the vicinity of ρ_c. This difference may originate in the fact that the transition fixed point T is only approximately described within the NLO approximation. It has, however, a negligible impact on the structure of the phase diagram.

In the strong-coupling sector, we find the two fixed points that govern the SR and LR rough phases, which constitutes our main result. They exchange their stability when LR comes across SR from an unphysical quadrant of the coupling space which occurs for $z_{\rm LR} = z_{\rm SR}$. We hence computed the phase boundary $\rho_{\rm SR}(d)$ which is not accessible within perturbation theory. All of the fixed points can be followed continuously when ρ and d are varied, and we show in particular that there exists a unique SR fixed point. This is not consistent with the scenario proposed by JFT of two SR phases, below and above $d_c(\rho)$ respectively, of different natures. We finally suggest that the RG finding does not in fact rule out the possibility that the SR phase (SR-I in JFT's work) has an upper critical dimension that differs from 4, and is possibly infinite, which would be compatible with the numerical results. However, the NLO approximation we used does not allow us to determine whether this possibility is realized within NPRG, as the NLO approximation does not allow us to accurately investigate the $d = 4$ case. This is left for future work.

ACKNOWLEDGMENTS

The authors acknowledges financial support from the ECOS-Sud France-Uruguay program U11E01. T.K. thanks the LPTMC at the Université Pierre et Marie Curie for hospitality, where parts of this work were achieved. T.K. also gratefully acknowledges financial support from the Alexander von Humboldt foundation, the IIP in Natal, and, for hospitality and computing resources, the group of P. Kopietz at the Goethe University Frankfurt. Finally, L.C. and B.D. thank the Universidad

de la República (Uruguay) for hospitality and the PEDECIBA for financial support during the completion of this work.

APPENDIX A: PERTURBATIVE ANALYSIS OF NPRG EQUATIONS

In this Appendix, we analyze the NPRG flow equations in some perturbative regimes. In the vicinity of $d = 2$ and $\rho = 0$, the NPRG flow equations coincide with Eqs. (4.33) and (4.34) of Ref. [38], which, in our normalizations, that is, with $u_{\rm JFT} = v_d \hat{g}_\kappa/2$, read as follows:

$$\partial_\kappa \hat{g}_\kappa = \hat{g}_\kappa \left[\epsilon - v_d \frac{\hat{g}_\kappa}{4}(1+\hat{w}_\kappa)^2 \right], \tag{A1a}$$

$$\partial_\kappa \hat{w}_\kappa = \hat{w}_\kappa \left[-2\rho + v_d \frac{\hat{g}_\kappa}{4}(1+\hat{w}_\kappa)^2 \right], \tag{A1b}$$

with $\epsilon = d - 2$.

The NPRG β functions for these couplings are given by Eqs. (21). The anomalous dimensions are defined at zero external momentum, through the normalization conditions $\hat{f}^v_\kappa(0) = \hat{f}^{\rm D}_\kappa(0) = 1$ ensuing from definitions (17) and (22). Equation (23) then yields the implicit equation for the anomalous dimensions

$$0 = \eta^X_\kappa + \hat{I}^X_\kappa(0), \tag{A2}$$

where both integrals $\hat{I}^v_\kappa(0)$ and $\hat{I}^{\rm D}_\kappa(0)$ depend linearly on η^v_κ and $\eta^{\rm D}_\kappa$. We hence define

$$\hat{I}^D_\kappa(0) = \hat{I}^{DD}_\kappa \eta^D_\kappa + \hat{I}^{Dv}_\kappa \eta^v_\kappa + \hat{I}^{D0}_\kappa, \tag{A3a}$$

$$\hat{I}^v_\kappa(0) = \hat{I}^{vD}_\kappa \eta^D_\kappa + \hat{I}^{vv}_\kappa \eta^v_\kappa + \hat{I}^{v0}_\kappa. \tag{A3b}$$

The explicit form of the various integrals is given by the following [22]:

$$\hat{I}^{DD}_\kappa = -\hat{g}_\kappa \frac{v_d}{2} \int_0^\infty d\hat{q}\, \hat{q}^{d+3} \frac{r(\hat{q}^2)\, \hat{k}_\kappa(\hat{q})}{\hat{f}^\lambda_\kappa(\hat{q})(\hat{l}_\kappa(\hat{q}))^3}, \tag{A4a}$$

$$\hat{I}^{Dv}_\kappa = \hat{g}_\kappa \frac{3v_d}{4} \int_0^\infty d\hat{q}\, \hat{q}^{d+5} \frac{r(\hat{q}^2)\, (\hat{k}_\kappa(\hat{q}))^2}{\hat{f}^\lambda_\kappa(\hat{q})(\hat{l}_\kappa(\hat{q}))^4}, \tag{A4b}$$

$$\hat{I}^{D0}_\kappa = \hat{g}_\kappa \frac{v_d}{2} \int_0^\infty d\hat{q}\, \frac{\hat{q}^{d+5}(\partial_{\hat{q}^2} r(\hat{q}^2))}{\hat{f}^\lambda_\kappa(\hat{q})(\hat{l}_\kappa(\hat{q}))^4} \hat{k}_\kappa(\hat{q}) \times [3\hat{q}^2 \hat{k}_\kappa(\hat{q}) - 2\hat{l}_\kappa(\hat{q})], \tag{A4c}$$

$$\hat{I}^{vD}_\kappa = \hat{g}_\kappa \frac{v_d}{4d} \int_0^\infty d\hat{q}\, \frac{\hat{q}^{d+1} r(\hat{q}^2)}{\hat{f}^\lambda_\kappa(\hat{q})(\hat{l}_\kappa(\hat{q}))^3} \times \left[\hat{f}^\lambda_\kappa(\hat{q}) \hat{q} \partial_{\hat{q}} \hat{l}_\kappa(\hat{q}) - \hat{l}_\kappa(\hat{q}) \hat{q} \partial_{\hat{q}} \hat{f}^\lambda_\kappa(\hat{q}) - 2\hat{f}^\lambda_\kappa(\hat{q}) \hat{l}_\kappa(\hat{q}) \right], \tag{A4d}$$

$$\hat{I}^{vv}_\kappa = -\hat{g}_\kappa \frac{v_d}{4d} \int_0^\infty d\hat{q}\, \frac{\hat{q}^{d+3} r(\hat{q}^2)}{\hat{f}^\lambda_\kappa(\hat{q})(\hat{l}_\kappa(\hat{q}))^3} \left[\hat{f}^\lambda_\kappa(\hat{q}) \hat{q} \partial_{\hat{q}} \hat{k}_\kappa(\hat{q}) - \left(2\hat{q} \partial_{\hat{q}} \hat{f}^\lambda_\kappa(\hat{q}) + (2-d) \hat{f}^\lambda_\kappa(\hat{q}) \right) \hat{k}_\kappa(\hat{q}) \right], \tag{A4e}$$

$$\hat{I}^{v0}_\kappa = -\hat{g}_\kappa \frac{v_d}{2d} \int_0^\infty d\hat{q}\, \frac{\hat{q}^{d+3} \partial_{\hat{q}^2} r(\hat{q}^2)}{\hat{f}^\lambda_\kappa(\hat{q})(\hat{l}_\kappa(\hat{q}))^3} \times \left[\hat{q} \partial_{\hat{q}} \hat{f}^\lambda_\kappa(\hat{q}) \left(-2\hat{q}^2 \hat{k}_\kappa(\hat{q}) + \hat{l}_\kappa(\hat{q}) \right) + \hat{f}^\lambda_\kappa(\hat{q}) \times \left(\hat{q}^3 \partial_{\hat{q}} \hat{k}_\kappa(\hat{q}) - \hat{q} \partial_{\hat{q}} \hat{l}_\kappa(\hat{q}) + (d-2) \hat{q}^2 \hat{k}_\kappa(\hat{q}) + 2\hat{l}_\kappa(\hat{q}) \right) \right], \tag{A4f}$$

where

$$\hat{k}_\kappa(\hat{q}) = \hat{f}^D_\kappa(\hat{q}) + \hat{w} \hat{q}^{-2\rho} + r(\hat{q}^2), \tag{A5a}$$

$$\hat{l}_\kappa(\hat{q}) = \hat{q}^2 \left(\hat{f}^v_\kappa(\hat{q}) + r(\hat{q}^2) \right). \tag{A5b}$$

[Note two misprints in Eqs. (A4d) and (A4f) of Ref. [22] corrected here].

To investigate the properties of the EWLR fixed points, we consider the limit $\hat{w} \to \infty$ and $\hat{g} \to 0$, at $\hat{g}\hat{w}^2$ fixed, that is, $\hat{x} \to 1$ at fixed $\hat{y}$. As long as $\hat{f}^v_\kappa$, $\hat{f}^D_\kappa$, and $\hat{f}^\lambda_\kappa$ are of order one in this limit (which holds by definition at LPA′ and is verified below at NLO), it amounts to replacing, in the various Eqs. (A4), $\hat{k}_\kappa(\hat{q})$ with $\hat{w}\hat{q}^{-2\rho}$. Accordingly, one observes that

$$\hat{I}^{DD}_\kappa = \mathcal{O}(\hat{y}/\hat{w}), \tag{A6a}$$

$$\hat{I}^{Dv}_\kappa = \mathcal{O}(\hat{y}), \tag{A6b}$$

$$\hat{I}^{D0}_\kappa = \mathcal{O}(\hat{y}), \tag{A6c}$$

$$\hat{I}^{vD}_\kappa = \mathcal{O}(\hat{y}/\hat{w}^2), \tag{A6d}$$

$$\hat{I}^{vv}_\kappa = \mathcal{O}(\hat{y}/\hat{w}), \tag{A6e}$$

$$\hat{I}^{v0}_\kappa = \mathcal{O}(\hat{y}/\hat{w}). \tag{A6f}$$

Let us check the behavior of the three functions $f^{\rm X}_\kappa$ in this limit in the NLO approximation. The NLO flow equations for the functions $\hat{f}^v_\kappa$, $\hat{f}^D_\kappa$, and $\hat{f}^\lambda_\kappa$ (see Ref. [22]) are of order

$$\partial_s \hat{f}^D_\kappa(\hat{q}) = \mathcal{O}(\hat{y}), \tag{A7a}$$

$$\partial_s \hat{f}^v_\kappa(\hat{q}) = \mathcal{O}(\hat{y}/\hat{w}), \tag{A7b}$$

$$\partial_s \hat{f}^\lambda_\kappa(\hat{q}) = \mathcal{O}(\hat{y}/\hat{w}). \tag{A7c}$$

As a consequence, in the limit $\hat{x} \to 1$ at fixed $\hat{y}$, one has indeed

$$\hat{f}^D_\kappa(\hat{q}) = \mathcal{O}(1), \tag{A8a}$$

$$\hat{f}^v_\kappa(\hat{q}) \to 1, \tag{A8b}$$

$$\hat{f}^\lambda_\kappa(\hat{q}) \to 1. \tag{A8c}$$

Therefore, even if $\hat{f}^D_\kappa$ does not remain at a bare level along the flow, the NLO and LPA′ expressions for the anomalous dimensions Eqs. (A2) in this limit are identical and become

$$\eta^D_\kappa = \rho \hat{y}_\kappa \tilde{\eta}^D(\rho, d), \quad \eta^v_\kappa = \rho \hat{y}_\kappa (1 - \hat{x}_\kappa) \tilde{\eta}^v(\rho, d), \tag{A9}$$

with

$$\tilde{\eta}^D(\rho, d) = -6 v_d \int_0^\infty d\hat{q}\, \frac{\hat{q}^{d-1-4\rho}(\partial_{\hat{q}^2} r(\hat{q}^2))}{[1 + r(\hat{q}^2)]^4}, \tag{A10a}$$

$$\tilde{\eta}^v(\rho, d) = \frac{2v_d}{d} \int_0^\infty d\hat{q}\, \frac{\hat{q}^{d-1-2\rho}(\partial_{\hat{q}^2} r(\hat{q}^2))\,(d - 2 - 2\rho)}{[1 + r(\hat{q}^2)]^3}. \tag{A10b}$$

Moreover the perturbative expansion of the NPRG flow equations for the couplings Eqs. (A1) in the variables $\hat{x}_\kappa$ and $\hat{y}_\kappa$ become

$$\partial_s \hat{x}_\kappa = \rho(\hat{x}_\kappa - 1)(2 - \tilde{\eta}^D(\rho, d) \hat{y}_\kappa) + \mathcal{O}(\hat{x}_\kappa - 1)^2, \tag{A11a}$$

$$\partial_s \hat{y}_\kappa = \hat{y}_\kappa (d - 2 + \rho(\tilde{\eta}^D(\rho, d) \hat{y}_\kappa - 4)) + \mathcal{O}(\hat{x}_\kappa - 1). \tag{A11b}$$

To study the stability of the EWLR fixed points, these flow equations can be linearized in the vicinity of a fixed point $(\hat{x}_*,\hat{y}_*)$ with $\hat{x}_* = 1$ and the corresponding stability matrix reads

$$\Omega = \begin{pmatrix} \frac{\partial(\partial_s \hat{x}_\kappa)}{\partial \hat{x}_\kappa} & \frac{\partial(\partial_s \hat{x}_\kappa)}{\partial \hat{y}_\kappa} \\ \frac{\partial(\partial_s \hat{y}_\kappa)}{\partial \hat{x}_\kappa} & \frac{\partial(\partial_s \hat{y}_\kappa)}{\partial \hat{y}_\kappa} \end{pmatrix} \Bigg|_{\hat{x}_\kappa=\hat{x}_*=1,\hat{y}_\kappa=\hat{y}_*}$$
$$= \begin{pmatrix} \rho(2-\hat{y}_*\tilde{\eta}^D) & 0 \\ \frac{\partial(\partial_s \hat{y}_\kappa)}{\partial \hat{x}_\kappa}\Big|_{\hat{x}_\kappa=1,\hat{y}_\kappa=\hat{y}_*} & d-2-4\rho+2\rho\hat{y}_*\tilde{\eta}^D \end{pmatrix}. \quad \text{(A12)}$$

To determine the component $\partial(\partial_s \hat{y}_\kappa)/\partial \hat{x}_\kappa$ requires to push the expansion (A11) of $\partial_s \hat{y}_\kappa$ to order $(\hat{x}_\kappa - 1)$, but this is not necessary for the study of the stability of fixed points with $\hat{x}_* = 1$. The expression (A12) of the stability matrix implies that for any fixed point with $\hat{x}_* = 1$, the two eigenvalues, which identify with the correction-to-scaling exponents, are $\omega_1 = \rho(2 - \hat{y}_*\tilde{\eta}^D)$ and $\omega_2 = d - 2 - 4\rho + 2\rho\hat{y}_*\tilde{\eta}^D$. We now discuss the two fixed points with $\hat{x}_* = 1$.

1. EWLR1 fixed point

The EWLR1 fixed point is located at $\hat{x}_* = 1$ and $\hat{y}_* = 0$. The corresponding correction-to-scaling exponents are

$$\omega_1 = 2\rho, \quad \omega_2 = \epsilon - 4\rho, \quad \text{(A13)}$$

which are identical to the correction-to-scaling exponents obtained by JFT [38,39]. Consequently, we recover the same stability conditions, namely the EWLR1 fixed point is always attractive in the $\hat{x}$ direction, whereas it is attractive in the $\hat{y}$ direction for $d > 2(1 + 2\rho)$ and repulsive for $d < 2(1 + 2\rho)$.

2. EWLR2 fixed point

The coordinates of the EWLR2 fixed point are

$$\hat{x}_* = 1, \quad \hat{y}_* = \frac{4}{\tilde{\eta}^D(\rho,d)}\left(1 - \frac{\epsilon}{4\rho}\right), \quad \text{(A14)}$$

and the corresponding correction-to-scaling exponents are given by

$$\omega_1 = \epsilon - 2\rho, \quad \omega_2 = 4\rho - \epsilon, \quad \text{(A15)}$$

which again identify with the correction-to-scaling exponents found perturbatively [38,39]. Checking that $\tilde{\eta}^D(\rho,d)$ is always positive, we deduce the same stability conditions as JFT. The EWLR2 fixed point is always attractive in the $\hat{x}$ direction, and EWLR1 and EWLR2 exchange their stability in the $\hat{y}$ direction when EWLR2 crosses EWLR1 at $d_{\mathrm{EWLR}} = 2(1 + 2\rho)$.

APPENDIX B: CUTOFF DEPENDENCE

In this Appendix, we discuss the dependence of our results in the regulator function, which can be tested *via* the variation of the (positive) parameter α in Eq. (9). Of course, physical observables computed from the exact NPRG equation (13) do not depend on the choice of regulator. However, any approximation induces a spurious dependence in this regulator, which can be used to test the quality of the approximation.

The α dependence of the critical exponent χ_{SR} of the SR fixed point at the NLO approximation has been studied in details in Ref. [22]. The exponent χ_{SR} is exact in $d = 1$ (no α-dependence) and depends very weakly on α in $d = 2$, with an optimal value of $\chi_{\mathrm{SR}} \simeq 0.373$, and somewhat more on α in $d = 3$, with an optimal value of $\chi_{\mathrm{SR}} \simeq 0.179$. In this work, we used $\alpha = 4$ in $d = 2,3$ which belongs to the interval in α where the variations of the critical exponents with this parameter are minimal, and their values very close to the optimal ones; see Ref. [22]. Increasing further the dimension above $d \gtrsim 3.5$, an increased cutoff dependence was observed, with even unphysical negative χ_{SR} values for small α in $d = 4$. This clearly signals that the NLO approximation becomes less accurate as the dimension grows and quantitatively unreliable for $d \gtrsim 3.5$. In particular, we here chose $\alpha = 10$ in $d = 4$ in order to get a positive exponent χ_{SR}, which is of the same order as the optimal value obtained at LO; see Ref. [22].

Let us now review the sensitivity of the results in the LR sector presented in this work with respect to a variation of the cutoff function, that is, of α. First, the boundary line $\rho_{\mathrm{SR}}(d)$ separating the LR and SR phases is entirely determined by the value of χ_{SR}, so its dependence on α can be directly inferred from that of χ_{SR} discussed above. Second, the critical exponents of the LR-dominated phases (EWLR1, EWLR2, and LR) are exact and thus independent of α. The same holds true for the correction-to-scaling exponents Eqs. (A13) and (A15) at the EWLR fixed points and thus for their stabilities. Indeed, only the coordinate $\hat{y}_*$ of EWLR2 depends on α through $\tilde{\eta}^{\mathrm{D}}$ [Eq. (A10)] and we checked that $\tilde{\eta}^{\mathrm{D}}$ remains positive for all values of α.

Finally, the coordinates of the LR, SR, and T fixed points do depend on α. However, below $d \simeq 3.5$, and also in $d = 4$, provided a sufficiently large value of α is chosen (to ensure that $\chi_{\mathrm{SR}} > 0$), the qualitative structure of the flow diagram with the relative positions of T, SR, and LR presented in Figs. 1, 2, and 4 is preserved, together with the stability change of SR and LR at $\chi_{\mathrm{SR}} = \chi_{\mathrm{LR}}$.

[1] M. Kardar, G. Parisi, and Y.-C. Zhang, Phys. Rev. Lett. **56**, 889 (1986).
[2] T. Halpin-Healy and Y.-C. Zhang, Phys. Rep. **254**, 215 (1995).
[3] J. Krug, Adv. Phys. **46**, 139 (1997).
[4] A. L. Barabási and H. E. Stanley, *Fractal Concepts in Surface Growth* (Cambridge University Press, Cambridge, UK, 1995).
[5] M. Prähofer and H. Spohn, J. Stat. Phys. **115**, 255 (2004).
[6] T. Sasamoto, J. Phys. A: Math. Gen. **38**, L549 (2005).
[7] T. Sasamoto and H. Spohn, J. Stat. Mech. (2010) P11013.
[8] P. Calabrese and P. Le Doussal, Phys. Rev. Lett. **106**, 250603 (2011).
[9] G. Amir, I. Corwin, and J. Quastel, Commun. Pure Appl. Math. **64**, 466 (2011).
[10] T. Imamura and T. Sasamoto, Phys. Rev. Lett. **108**, 190603 (2012).
[11] I. Corwin, Random Matrices **01**, 1130001 (2012).

[12] K. A. Takeuchi and M. Sano, Phys. Rev. Lett. **104**, 230601 (2010).
[13] K. A. Takeuchi, M. Sano, T. Sasamoto, and H. Spohn, Sci. Rep. **1**, 34 (2011).
[14] K. Takeuchi and M. Sano, J. Stat. Phys. **147**, 853 (2012).
[15] J. Kelling and G. Ódor, Phys. Rev. E **84**, 061150 (2011).
[16] A. Pagnani and G. Parisi, Phys. Rev. E **87**, 010102 (2013).
[17] T. Halpin-Healy, Phys. Rev. Lett. **109**, 170602 (2012).
[18] T. Halpin-Healy, Phys. Rev. E **88**, 042118 (2013); **88**, 069903(E) (2013).
[19] T. J. Oliveira, S. G. Alves, and S. C. Ferreira, Phys. Rev. E **87**, 040102 (2013).
[20] L. Canet, H. Chaté, B. Delamotte, and N. Wschebor, Phys. Rev. Lett. **104**, 150601 (2010).
[21] L. Canet, H. Chaté, B. Delamotte, and N. Wschebor, Phys. Rev. E **84**, 061128 (2011); **86**, 019904(E) (2012).
[22] T. Kloss, L. Canet, and N. Wschebor, Phys. Rev. E **86**, 051124 (2012).
[23] L.-H. Tang, B. M. Forrest, and D. E. Wolf, Phys. Rev. A **45**, 7162 (1992).
[24] T. Ala-Nissila, T. Hjelt, J. M. Kosterlitz, and O. Venäläinen, J. Stat. Phys. **72**, 207 (1993).
[25] C. Castellano, M. Marsili, M. A. Muñoz, and L. Pietronero, Phys. Rev. E **59**, 6460 (1999).
[26] E. Marinari, A. Pagnani, and G. Parisi, J. Phys. A: Math. Gen. **33**, 8181 (2000).
[27] F. D. A. Aarão Reis, Phys. Rev. E **69**, 021610 (2004).
[28] S. V. Ghaisas, Phys. Rev. E **73**, 022601 (2006).
[29] M. A. Rubio, C. A. Edwards, A. Dougherty, and J. P. Gollub, Phys. Rev. Lett. **63**, 1685 (1989).
[30] V. K. Horvath, F. Family, and T. Vicsek, J. Phys. A: Math. Gen. **24**, L25 (1991).
[31] P. Meakin and R. Jullien, Europhys. Lett. **9**, 71 (1989).
[32] H. G. E. Hentschel and F. Family, Phys. Rev. Lett. **66**, 1982 (1991).
[33] J. G. Amar, P.-M. Lam, and F. Family, Phys. Rev. A **43**, 4548 (1991).
[34] C.-K. Peng, S. Havlin, M. Schwartz, and H. E. Stanley, Phys. Rev. A **44**, R2239 (1991).
[35] N.-N. Pang, Y.-K. Yu, and T. Halpin-Healy, Phys. Rev. E **52**, 3224 (1995).
[36] M. S. Li, Phys. Rev. E **55**, 1178 (1997).
[37] S. Mukherji and S. M. Bhattacharjee, Phys. Rev. Lett. **79**, 2502 (1997).
[38] H. K. Janssen, U. C. Täuber, and E. Frey, Eur. Phys. J. B **9**, 491 (1999).
[39] E. Frey, U. C. Täuber, and H. K. Janssen, Europhys. Lett. **47**, 14 (1999).
[40] E. Katzav and M. Schwartz, Phys. Rev. E **60**, 5677 (1999).
[41] M. K. Verma, Physica A **277**, 359 (2000).
[42] E. Katzav, Phys. Rev. E **68**, 046113 (2003).
[43] E. Katzav, Physica A **392**, 1750 (2013).
[44] E. Medina, T. Hwa, M. Kardar, and Y.-C. Zhang, Phys. Rev. A **39**, 3053 (1989).
[45] C.-H. Lam, L. M. Sander, and D. E. Wolf, Phys. Rev. A **46**, R6128 (1992).
[46] E. Katzav and M. Schwartz, Phys. Rev. E **69**, 052603 (2004).
[47] A. A. Fedorenko, Phys. Rev. B **77**, 094203 (2008).
[48] T. Halpin-Healy, Phys. Rev. A **42**, 711 (1990).
[49] Y.-C. Zhang, Phys. Rev. B **42**, 4897 (1990).
[50] F. Hayot and C. Jayaprakash, Phys. Rev. E **54**, 4681 (1996).
[51] J. K. Bhattacharjee, J. Phys. A: Math. Gen. **31**, L93 (1998).
[52] C. Castellano, M. Marsili, and L. Pietronero, Phys. Rev. Lett. **80**, 3527 (1998).
[53] H.-K. Janssen, Z. Phys. B **23**, 377 (1976); C. de Dominicis, J. Phys. (Paris), Colloq. **37**, 247 (1976).
[54] P. C. Martin, E. D. Siggia, and H. A. Rose, Phys. Rev. A **8**, 423 (1973).
[55] V. V. Lebedev and V. S. L'vov, Phys. Rev. E **49**, R959 (1994).
[56] L. Canet, H. Chaté, and B. Delamotte, J. Phys. A **44**, 495001 (2011).
[57] J. Berges and D. Mesterházy, Nucl. Phys. B Proc. Suppl. **228**, 37 (2012).
[58] P. Kopietz, L. Bartosch, and F. Schütz, *Introduction to the Functional Renormalization Group*, Lecture Notes in Physics (Springer, Berlin, 2010).
[59] J. Berges, N. Tetradis, and C. Wetterich, Phys. Rep. **363**, 223 (2002).
[60] B. Delamotte and L. Canet, Condens. Matter Phys. **8**, 163 (2005).
[61] F. Benitez and N. Wschebor, Phys. Rev. E **86**, 010104 (2012).
[62] B. Delamotte, in *Renormalization Group and Effective Field Theory Approaches to Many-Body Systems*, edited by J. Polonyi and A. Schwenk, Lecture Notes in Physics (Springer, Berlin, 2012); B. Delamotte, arXiv:cond-mat/0702365 (2007).
[63] C. Wetterich, Phys. Lett. B **301**, 90 (1993).
[64] J.-P. Blaizot, R. Méndez-Galain, and N. Wschebor, Phys. Lett. B **632**, 571 (2006).
[65] F. Benitez, J.-P. Blaizot, H. Chaté, B. Delamotte, R. Méndez-Galain, and N. Wschebor, Phys. Rev. E **80**, 030103 (2009).
[66] F. Benitez, J.-P. Blaizot, H. Chaté, B. Delamotte, R. Méndez-Galain, and N. Wschebor, Phys. Rev. E **85**, 026707 (2012).
[67] L. Canet, arXiv:cond-mat/0509541.
[68] In $d = 4$, we choose the cutoff parameter $\alpha = 10$, see Appendix B.
[69] D. Forster, D. R. Nelson, and M. J. Stephen, Phys. Rev. A **16**, 732 (1977).